Incorporating Coverage-dependent Reaction Barriers into First-principles Based Microkinetic Models: Approaches and Challenges

Michelle A. Nolen[1,2], Carrie A. Farberow[1*], and Stephanie Kwon[2*]

[1]Catalytic Carbon Transformation & Scale-Up Center, National Renewable Energy Laboratory, Golden, Colorado 80401, United States

[2]Department of Chemical and Biological Engineering, Colorado School of Mines, Golden, Colorado 80401, United States

** Corresponding authors: Carrie.Farberow@nrel.gov, kwon@mines.edu*

Keywords: microkinetic modelling, coverage effects, transition states, density functional theory, heterogeneous catalysis

Abstract

Mean-field microkinetic models are appealing for their relatively facile construction, computational tractability, and high-throughput catalyst screening capabilities. As such, they will continue to be a valuable tool for materials design in heterogeneous catalysis even as the field aims to describe more complex systems. Numerous prior reports have provided groundwork for constructing first-principles based microkinetic models, including analysis of strategies for incorporating lateral interactions into thermodynamic parameters (e.g., adsorption energies). Yet, there remains a need for concerted dialogue on strategies for calculating and incorporating coverage-dependent kinetic parameters into microkinetic models. In this perspective, we assess strategies for doing so, including the corresponding key physical implications and computational challenges. We emphasize that decoupling thermodynamic and kinetic parameters within a microkinetic model can violate thermodynamic consistency and risks unphysical solutions. For some reactions and catalyst materials, scaling relationships can predict coverage-dependent activation energies, but there are several exceptions evident in the literature indicating that this approach is not universally applicable, and that the field could benefit from research aimed at elucidating the limitations. Conducting high-coverage transition-state searches is a rigorous but computationally costly strategy, and the effects of various methods for mitigating this cost on resulting energetics have yet to be broadly explored and validated. The goal of this perspective is to generate discussion on and inspire focused research into the physical relevance of approaches for describing coverage-dependent reaction barriers in microkinetic models, including the development of computationally tractable methodologies, to advance the applicability of MKMs across diverse reaction chemistries and conditions.

1. Introduction

Mean-field microkinetic models (MKMs) are widely used to evaluate reaction mechanisms and screen catalytic materials in the field of heterogeneous catalysis.[1–5] These models are comprised of a set of differential equations that describe the evolution of surface-bound and gas-phase intermediate concentrations in a predefined reaction network. Solutions are obtained by solving the system of equations for a given time span or reactor length with a set of initial conditions. Post-solution processing enables predictions of macroscale catalytic performance (i.e., rates, selectivities) and kinetic behaviors (i.e., rate laws, apparent activation energy barriers), while providing insights on reaction mechanisms (i.e., sensitivity analysis, dominant reaction pathways). Under the mean-field approximation, all sites are treated identically, and there are no spatial correlations between sites; model solutions are averaged across species' surface concentrations.

A fundamental feature of MKMs is the required parametrization of reaction energetics for elementary steps in the reaction network, often achieved using first-principles calculations based on density functional theory (DFT). The DFT-derived energies are often provided as energies of transition-state (TS) complexes and adsorption energies of surface-bound reaction intermediates on the catalyst surface of interest. Corresponding activation energy barriers and reaction free energies, and rate and equilibrium constants, are then calculated within the MKM code.[2,6] Due to the exponential nature of rate and equilibrium constants, MKM solutions can vary significantly even with small (i.e., 0.01 eV) perturbations in a few of the DFT-derived parameters (i.e., sensitive parameters). If available, the model predictions can be compared with experimental data to confirm the accuracy of the model. Ultimately, MKMs facilitate mechanistic connections between atomic-scale models and macroscale observations.

The aforementioned parameter sensitivity necessitates the careful selection of atomic-scale modelling parameters, driven by an understanding of the corresponding physical implications. As such, active site models are typically designed to reflect certain physical properties of the catalyst. In this perspective, we focus our discussions on slab models with periodic boundary conditions that aim to describe catalysis on large surfaces of metals, metal-oxides, metal-sulfides, etc. For example, large metal nanoparticles (> 5 nm) are conventionally represented by periodic slab models of the most thermodynamically stable facet, which is primarily exposed. In contrast, stepped surfaces or nanocluster models are often employed to represent the undercoordinated sites on a smaller nanoparticle size;[7] models that target more structurally complex catalyst materials, such as porous catalysts, are beyond the scope of this discussion. For slab models with periodic boundary conditions, the use of large periodic unit cells represents a dilution of surface intermediates. Correspondingly, smaller unit cells correspond to a denser surface concentration. Monolayer (ML) coverage is conventionally defined as the number of adsorbates per

surface site; for example, one adsorbate in a 2 × 2 supercell with four surface metal atoms is denoted as 1/4 ML; the topic of unit cell size is further discussed in **Section 2.3.2a**.

Indeed, the quantity and configuration of surface-bound intermediates in periodic models are nontrivial parameters. When surface intermediates are expected to be present at significant coverages during catalytic turnovers, as predicted by spectroscopy or a steady-state MKM simulation solution, it becomes necessary to incorporate most-abundant surface intermediates (MASIs) on the model active sites, thereby capturing the effects of adsorbate-adsorbate or lateral interactions on the adsorption energies of intermediates and TSs (i.e., coverage effects). Such high-coverage systems are relevant to diverse chemistries important to addressing energy and environmental challenges, including NO oxidation/reduction,[8,9] CO oxidation/hydrogenation,[10–13] formic acid decomposition,[14,15] and methanol synthesis[16]. We note that conventional mean-field simulations cannot consider spatial configurations of accumulating adsorbates that may influence system dynamics; we refer readers to the substantial prior research devoted to describing configurations of adsorbates with non-mean-field MKMs.[17–24] Lattice-based kinetic Monte Carlo (kMC) simulations allow for configuration-dependent rate expressions and descriptions of correlations between sites, but they are generally only computationally tractable for simple reaction networks, with a computational cost nearly three orders of magnitude larger than that of MKMs.[1] As such, MKMs remain an attractive option for relatively facile, high-throughput modelling, especially for systems characterized by complex reaction networks.

In recent years, implementing coverage-dependent energetics into MKMs is increasingly common, as the field attempts to understand and describe the role of the reaction microenvironment.[16,19,25–29] Incorporating adsorbate-adsorbate interactions into a surface model often nonuniformly influences the calculated stabilities of intermediates and TSs, resulting in reaction energies and activation barriers that can deviate nonmonotonically from those calculated at ideal, low-coverage conditions even by more than 1 eV.[8,9,26,30,31] Coverage-cognizant energetics in an MKM can therefore significantly impact model solutions, including changes in i) the identity of the kinetically relevant steps, which are reflected in sensitivity/degree of rate control analysis, ii) the dominant reaction route, reflected in reaction flux analysis, and/or iii) the overall apparent activation energy (E_{app}), reflected in the change in turnover frequencies (TOFs) with temperature. [4,10–12,25,26,28,31–34]

Here, we discuss the challenges in capturing the effects of adsorbate-adsorbate interactions on kinetic parameters in MKMs. In these models, the changes in coverage-dependent energetic parameters propagate throughout the hierarchical structure of the MKM equations, beginning with coverage-dependent adsorption energies, to reaction energies, and finally, to activation barriers. Numerous prior works by Grabow, Dumesic, Mavrikakis, Schneider, Nørskov, and others provide significant groundwork for guiding the construction of steady-state MKMs,[1–3,6,13,17,35–37] including works focused on the design of equations

that describe coverage-dependent thermodynamic parameters (e.g,. adsorption and reaction energies).[8,13,25,38,39] However, connections between coverage-induced changes in thermodynamic and kinetic parameters (e.g., activation barriers) for elementary steps have not been previously discussed in detail, despite the significant consequences on the model solutions.

In this perspective, we detail the mathematical equations corresponding to coverage-induced changes in energetic parameters within bottom-up (DFT-parametrized, or first-principles based) MKMs, and discuss the corresponding implications on the reaction kinetics. We provide a systematic assessment of the common techniques applied in the literature for describing coverage-dependent kinetic parameters within MKMs, including the validity of their accompanying physical implications, and the relative computational tractability. The goal is to provide clarity and generate discussion on the current strategies and challenges involved in calculating coverage-dependent rate constants, and to inspire transparency in reporting methods used and the development of improved approaches. The topics discussed herein are relevant to any MKMs with DFT-derived parameters that aim to capture the effects of lateral interactions on reaction energies and activation barriers.

2. Discussion

2.1 Hierarchical connections between coverage-dependent equations within DFT-parametrized MKMs

Periodic DFT calculations are often designed to simulate low-coverage conditions, where each adsorbate is infinitely separated, and adsorbate-adsorbate interactions are negligible. This approximation is appealing for its low computational cost, relatively facile model construction, and may appropriately represent some catalytic systems where species are unlikely to accumulate on the surface (e.g., systems under sufficiently high temperatures, low reactant pressures, or those that use catalyst materials with weak binding affinities). For catalysts that experience higher adsorbate coverages during catalytic turnovers – as indicated by kinetic and spectroscopic data, or steady-state model solutions – lateral interactions are expected to influence DFT-derived energies.

Equations 1-6 demonstrate the relationship between reaction energies, adsorption energies, and activation barriers typically used in MKM formulations. Adsorption energies are typically defined as:

$$E_{ads,j} = E_{j+surface} - E_{surface} - E_{j(g)} \quad (1)$$

Here, $E_{ads,j}$ is the adsorption energy of a bound intermediate *j* (adsorbate), $E_{j+surface}$ is the total energy of the adsorbate *j* bound to the surface, $E_{surface}$ is the energy of the surface, and $E_{j(g)}$ is the energy of the corresponding gas-phase (unbound) intermediate.

Reaction energies are defined as the difference in energy between reactant and product energies. In the case of surface reactions, these terms can be calculated by summing the adsorption energies and gas-phase energies of the respective states (**Eqn. 2**).

$$\Delta E_{rxn,i} = \Sigma E_{products} - \Sigma E_{reactants}$$
$$= \Sigma E_{ads,\ products} + \Sigma E_{gas,\ products} - (\Sigma E_{ads,\ reactants} + E_{gas,\ reactants}) \quad (2)$$

Here, $\Delta E_{rxn,i}$ is the reaction energy of elementary step *i* and $E_{products}$, and $E_{reactants}$ are the energies of the reactants and products of the elementary step. $E_{ads,\ products}$ and $E_{ads,\ reactants}$ are the adsorption energies of the products and reactants, respectively, and $E_{gas,\ products}$ and $E_{gas,\ reactants}$ are the gas-phase energies of the products and reactants, respectively. The activation energy barriers are calculated as the difference between the transition state energy and the reactants (forward barrier, $E_{a,f}$) or products (reverse barrier, $E_{a,r}$):

$$E_{a,f} = E_{TS} - \Sigma E_{ads,\ reactants} - \Sigma E_{gas-phase,\ reactants} \quad (3)$$

$$E_{a,r} = E_{TS} - \Sigma E_{ads,\ products} - \Sigma E_{gas-phase,\ products} \quad (4)$$

$$\Delta E_{rxn} = E_{a,f} - E_{a,r} \quad (5)$$

Upon the calculation of vibrational frequencies, the energies of adsorbates and TSs can be temperature-corrected via statistical mechanical formalisms[40] to provide the respective free energy values. The free energy barriers are then used to calculate rate constants of an elementary step *i* (**Eqn. 6-7**) based on TS theory:[41]

$$k_{i,f} = \frac{k_B T}{h} \exp\left[\frac{-G_{a,f}}{RT}\right] \quad (6)$$

Here, $k_{i,f}$ and $G_{a,f}$ are the forward rate constant and activation barrier for a reversible elementary step *i*. k_B, T, h, and R are Boltzmann's constant, temperature, Planck's constant, and the ideal gas constant, respectively. $K_{eq,i}$, the equilibrium constant of the elementary step, is calculated from the corresponding reaction free energy $\Delta G_{rxn,i}$:

$$K_{eq,i} = \exp\left[\frac{-\Delta G_{rxn,i}}{RT}\right] \quad (7)$$

The magnitude of the reverse activation barrier ($G_{a,r}$) and the corresponding rate constant ($k_{i,r}$) are often calculated implicitly from $K_{eq,i}$ amd $k_{i,f}$, to maintain thermodynamic consistency (i.e., **Eqn. 5**):

$$k_{i,r} = \frac{k_{i,f}}{K_{eq,i}} \quad (8)$$

We note here that we implement the common equations for defining rate constants, equilibrium constants, and rate equations in microkinetic models,[2,6] although we refer the interested reader to prior works

discussing formal definitions with respect to standard states.[42–44] Thus, when $\Delta G_{rxn,i}$ (and therefore $K_{eq,i}$; **Eqn. 7**) changes as a function of coverage, $k_{i,r}$ and/or $k_{i,f}$ must also change proportionally, as dictated by **Eqn. 5** and **8**. We focus our discussion on the electronic components of the free energies (i.e., $E_{a,f}$, $E_{a,r}$, and ΔE_{rxn}), which comprise the dominant portion of free energies at low to moderate temperatures, although we recognize that adsorbate-adsorbate interactions can influence vibrational frequencies and, consequently, temperature-corrected values (*ZPE*, *H*, *S*).[45–47] Furthermore, the frequencies are often calculated under the harmonic approximation, which is known to introduce errors in vibrational frequency analysis, especially for low modes that arise from weakly-bound species.[48] Thus, further research is needed to define best practices in the field for performing vibrational frequency analysis in the presence of spectator species.

For each elementary step *i*, the forward ($r_{i,f}$) and reverse ($r_{i,r}$) rate are determined by the fractional surface coverages of the reactants and products (θ_j, where $0 \leq \theta_j \leq 1$) and forward and reverse rate constants ($k_{i,f}$ and $k_{i,r}$, respectively) for the elementary step:

$$r_{i,f} = k_{i,f} \prod [\theta_j]^{\nu_{ij}} \tag{9}$$

$$r_{i,r} = k_{i,r} \prod [\theta_j]^{\nu_{ij}} \tag{10}$$

Here, ν_{ij} is the stoichiometric coefficient of an intermediate *j* as determined by the balanced elementary step *i*. Note that the polynomial site dependencies of rates (**Eqns. 9 and 10**) rely upon the assumptions of fast-diffusion and consequently randomized adsorbate distributions, and that divergence from this behavior is possible when there are site occupancy correlations.[18] In fact, the assignment of "surface sites" is a nontrivial task; conventional MKMs assume a simple site balance equation, where the total number of active sites is often quantified as the number of surface atoms in a specified area (unit cell). In general, the surface species *j* occupies a single active site; thus, the fractional coverages of intermediates, including vacant sites, must sum to one. Distinct from this definition, active sites assignments in DFT calculations typically refer to unique high-symmetry adsorption sites of a faceted surface (e.g., top vs. hollow sites on a (111) facet). Previous reports have proposed the use of two-site models to describe 'reservoirs' of adsorbates that do not competitively adsorb on the same high-symmetry site as the remaining adsorbates,[16,49] or when the surface has two distinct types of active sites (e.g., metal and oxygen atoms in metal-oxides).[50] Larger adsorbates can be defined as occupying more than one of these sites, depending on their binding mode (i.e., monodentate vs. bidentate).[51] We refer readers to literature addressing the complex task of site assignments and balances in heterogeneous catalysis.[18,22,32,52] Such topics are critical in forming accurate predictions of θ_j, and consequently, rates of elementary steps.

According to the law of mass action, the net rate of an elementary step ($r_{net,i}$) is then written as:

$$r_{net,i} = r_{i,f} - r_{i,r} \tag{11}$$

The net rates are used to calculate the time- or volume-dependent mole balances of each species, describing the change in surface concentration of a given intermediate for transient CSTRs (**Eqn. 12a)** or PFRs (**Eqn. 12b**), respectively:

$$\frac{\partial \theta_j}{\partial t} = \sum \nu_{ij} r_{net,i} \tag{12a}$$

$$\frac{\partial F_j}{\partial V} = \sum \nu_{ij} r_{net,i} \tag{12b}$$

The time-dependent mole balances make up the system of ordinary differential equations (ODEs) solved within the MKM for a specified time span in a transient CSTR – ideally, a time span sufficiently long to capture steady-state behavior. The solutions to the converged model are so-called *steady-state* concentrations, which are used in post-solution processing to quantify the macroscopic kinetics. The steady-state solutions to a transient CSTR model at differential conversions can be used as initial guesses to describe reaction kinetics in a PFR. In this case, the PFR is described by a system of differential algebraic equations (DAEs), where species' concentrations evolve over the reactor length (rather than time) (**Eqn. 12b**). Transient CSTRs are commonly employed in microkinetic models as the system of ODEs are easier to converge than the system of DAEs for PFR models.[51] Steady-state rates can be validated against experimental kinetic data from flow reactors with small bed volumes, operated at low (differential) conversions.[2] We refer readers to the thorough review by Dumesic and coworkers[2] for further details regarding the MKM equations for both CSTR and PFR models, and the construction of steady-state MKMs, as well as an introductory guidebook authored by Filot,[6] and additional resources.[1,36,37,53] A simplified workflow of the conventional microkinetic modelling process, adapted from Bhandari et al.,[36] is shown in **Figure 1**.

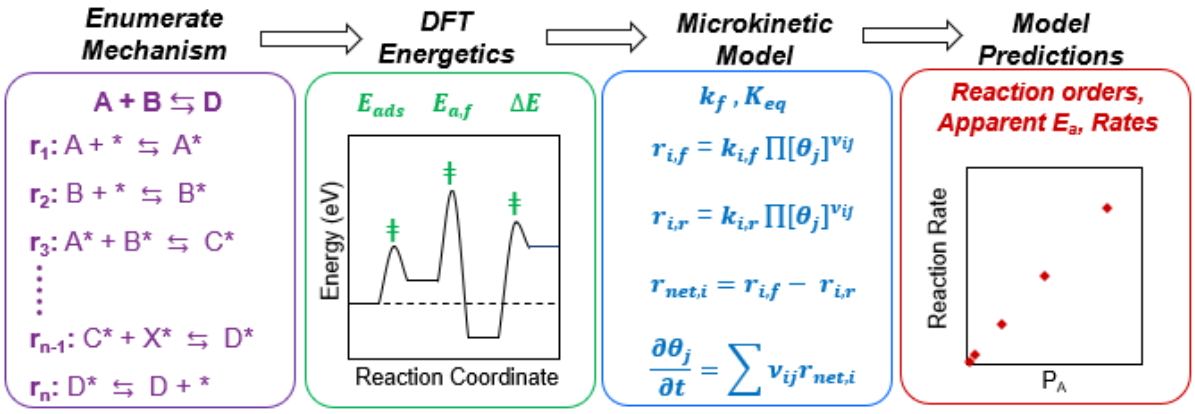

Figure 1. Schematic representation of the typical workflow adopted in the formulation and analysis of a first-principles based microkinetic model, **adapted from**[36]. Copyright 2020 American Chemical Society.

The topics discussed herein address the impacts of coverage-induced changes on the parameters in **Eqns. 1-8**, and are thus applicable to either transient CSTR or PFR models. To maintain reasonable computational cost in parameterizing coverage-cognizant models, it is commonplace to only consider lateral interactions induced by the most prevalent MASIs.[1,8,15,16,29,53,54] Within the MKM code, the adsorption energies of selected intermediates are written as functions of at least one species' surface concentration ($E_{ads,j}= f(\theta_m)$, where m may or may not be equal to j). Any adsorption energies that are defined as a function of θ_m are adjusted iteratively as the MKM solves the system of differential equations. Inherently, the changes in coverage-dependent $E_{ads,j}$ affect reaction energies (**Eqn. 2**) and activation barriers (**Eqns. 3-4**), and thus rate and equilibrium constants (**Eqns. 6-8**). These will affect the calculation of rates and ODE/DAE solutions (**Eqns. 9-12**).

2.2 Incorporating coverage-dependent thermodynamics and kinetics in MKMs

To further detail the connection between coverage-dependent thermodynamic and kinetic parameters, consider a single elementary reaction step involving three surface intermediates (A*, B*, and C*, * indicates a bound species), on a catalytic surface with significant fractional coverages of A* (θ_{A*}):

$$A* + B* \leftrightarrows C* + * \qquad R(1)$$

In this example, the adsorption energies of surface-bound intermediates ($E_{ads,A*}$, $E_{ads,B*}$ and $E_{ads,C*}$) depend on the coverage of A*, as described by coverage-dependent functions within the MKM:

$$E_{ads,j} = f(\theta_{A*}) \qquad (13)$$

Here, j is either A*, B*, or C*. Parametrizing this equation typically involves calculating the adsorption energies of adsorbates at incremental concentrations of spectator species, and fitting the data to a curve, [25,53] or alternatively, generating a cluster expansion.[4,33] We refer readers to a prior study by Schneider and coworkers devoted to the development of different mathematical expressions of **Eqn. 13**, including linear, piecewise, and activity-based models,[25] and a prior report by Hu and coworkers that detailed the use of a one- or two-line model to describe changes in adsorption energy as a function of coverage.[53] As the MKM iteratively solves the mole balances of surface species (**Eqn. 12**), θ_{A*} – and consequently $E_{ads,A*}$, $E_{ads,B*}$ and $E_{ads,C*}$ – are updated. According to **Eqn. 2**, the surface reaction energy for the example surface reaction (**R1**) is modified as:

$$\Delta E_{rxn}(\theta_{A*}) = E_{ads,C*}(\theta_{A*}) - (E_{ads,A*}(\theta_{A*}) + E_{ads,B*}(\theta_{A*})) + \Delta E_{rxn,A(g)+B(g)\rightarrow C(g)} \qquad (14)$$

This equation demonstrates how coverage-induced changes in E_{ads} of A*, B*, or C* lead to a change in ΔE_{rxn}.

To maintain thermodynamic consistency of an elementary step (i.e., satisfy **Eqn. 5**), either the forward, reverse, or both activation barriers must also change with the change of ΔE_{rxn}. Consider the base

case of a coverage-independent reaction profile of a single elementary step (black lines, **Scheme 1**), where all energies are defined relative to a reference state (E_{ref}; commonly the reactants in the gas-phase). The initial- and final-state energies (E_{IS} and E_{FS}, respectively) reflect the energy of the reactants and products on the catalyst surface, connected by the transition state (E_{TS}) along the reaction coordinate. We address three different cases (**Scheme 1a-1c,** dashed lines) illustrative of scenarios resultant from implementing coverage-induced changes to the kinetic parameters alongside a coverage-induced change in ΔE_{rxn}. These are briefly described in the documentation for the open-source descriptor-based MKM screening software package, CatMAP, developed by Nørksov and coworkers.[37] We elaborate here on the implementation, important considerations, and limitations of each case. For the purpose of illustration, these examples are presented assuming that the lateral interactions are destabilizing; that is, the energies of coverage-dependent surface bound intermediates become more positive (less favorable) with increasing surface coverage, although stabilizing lateral interactions are also possible.[16]

(i) The activation energy barrier in one direction (i.e., $E_{a,f}$ or $E_{a,r}$) is defined as a constant, coverage-independent value. The change in ΔE_{rxn} results in a change in the other (i.e., non-constant) barrier of the same magnitude. E_{TS} shifts correspondingly (**Scheme 1a**).

(ii) E_{TS} is defined as a constant, coverage-independent value. The change in ΔE_{rxn} results in changes in the magnitudes of both $E_{a,f}$ (calculated via **Eqn. 3**) and $E_{a,r}$ (calculated via **Eqn. 4**), where the sum of the change in magnitude of the elementary step barriers is equal to the change in ΔE_{rxn} such that **Eqn. 5** is satisfied (**Scheme 1b**).

(iii) E_{TS} or one activation energy barrier (e.g., $E_{a,f}$) is described by a coverage-dependent equation or determined from first-principles calculations at a representative high coverage (**Scheme 1c**). The remaining parameter, (e.g., $E_{a,r}$) is determined from **Eqn. 4** or **Eqn. 5,** which should give the same value, maintaining thermodynamic consistency.

Case i or ii arises when coverage-dependent adsorption energies are implemented without the corresponding inclusion of a coverage dependency for transition state energies (or activation barriers). These cases for a single elementary step are described in **Schemes 1a and 1b**, respectively, compared with the original profile of the elementary step at low coverage (solid black lines in **Scheme 1**). These figures show how cases (i) and (ii) can lead to dramatic changes in forward (and/or reverse) activation barriers with significant consequences in MKM solutions. While many previous reports describe the methods for incorporating coverage-dependent adsorption energies (and thus reaction energies) into an MKM, the methods for incorporating coverage-dependent E_{TS} or $E_{a,f}$ are often less detailed. As activation barriers are inherently correlated with adsorption energies within the MKM code, as we show here, it is possible

that scenario (i) or (ii) is implemented unintentionally without careful consideration. We thus discuss these cases to better inform those new to the field, where the consequences and implications of these scenarios may not be immediately intuitive, and to highlight the opportunity to improve consistency in documentation.

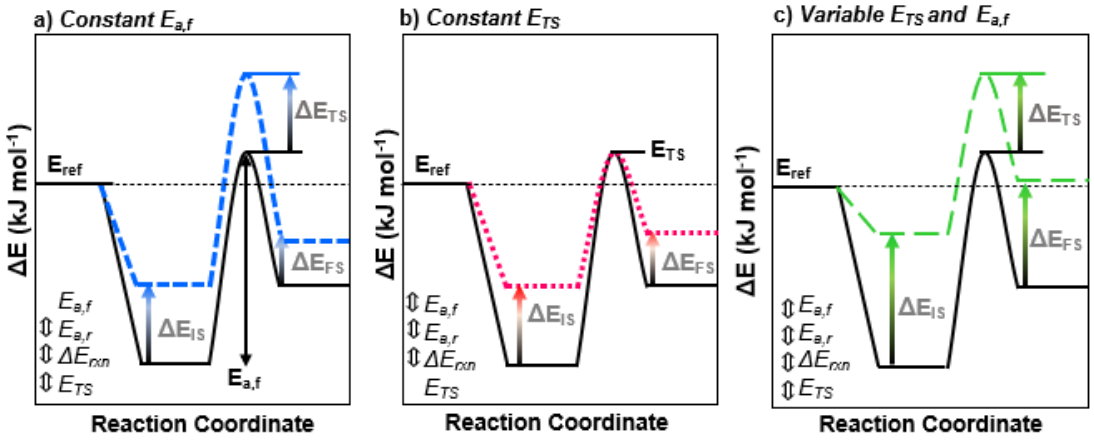

Scheme 1: Representative coverage-induced changes in the reaction energy profile of a single elementary step, relative to the original profile (solid black lines). $E_{a,f}$ or E_{TS} are treated as constant values to generate the high-coverage blue (a) and red (b) profiles; both $E_{a,f}$ and E_{TS} change to generate the high-coverage green (c) profile. A change (⇳) in the relevant parameters is indicated in the bottom left of each profile. E_{IS}, E_{FS}, $E_{a,f}$, $E_{a,r}$, and E_{TS} indicate the initial-state energy, final-state energy, forward activation barrier, reverse activation barrier, and TS energy relative to the reference state (E_{ref}), respectively.

The first case (**Scheme 1a**) assumes that the activation barrier in one direction is unaffected by lateral interactions, thereby defining the barrier as a constant parameter within the MKM. For clarity, the discussion that follows assumes that the fixed barrier is the forward barrier. If $E_{a,f}$ is defined as a constant in the MKM, E_{TS} and $E_{a,r}$ are altered to accommodate coverage-induced changes in ΔE_{rxn} (**Scheme 1a**) and maintain thermodynamic consistency (**Eqn. 5**). This may lead to erroneous results if, for example, a coverage-dependent ΔE_{rxn} exceeds the fixed magnitude of $E_{a,f}$. In such a scenario, $E_{a,r}$ becomes negative to satisfy **Eqn. 5**. In addition, accounting for the full magnitude of the change in ΔE_{rxn} through $E_{a,r}$ can greatly influence the net rate of an elementary step, particularly if the change in ΔE_{rxn} is significant.

Instead of a fixed activation barrier, case ii (**Scheme 1b**) imposes the requirement that E_{TS} is constant with varying coverage. This restriction inherently results in changes to the activation barrier magnitudes because of the mathematical constraints of the model (**Eqns. 2-5**). Depending on the magnitude of the change in the initial state and final state energies, this approach can likewise lead to large changes in barriers and thereby the predicted net rates of elementary steps.

We thus emphasize that adsorption energies cannot change independent of activation barriers in a thermodynamically consistent MKM. As such, for both cases (i) and (ii), which involve fixing a single kinetic parameter, it is important to consider the physical implications and relevance of the resulting parameter changes. That is, are the changes in the forward and reverse rates, and thus net rates, reasonable and consistent with the expected effects of increased coverage. Ultimately, implementing coverage-dependent thermodynamic parameters (E_{ads} , ΔE_{rxn}, K_{eq}) while neglecting to design coverage-dependent kinetic parameters ($E_{a,f}$ and/or E_{TS}, k) imposes the assumption that only stable intermediates, and not TSs, are influenced by lateral interactions, and risks unphysical steady-state solutions.

Case (iii) involves calculations of TS energies as a function of adsorbate coverage. Such a task, however, is not trivial and can be computationally demanding, especially given the challenges of performing high-coverage DFT calculations. Simplifying the atomic-scale models used to conduct TS searches or estimating activation barriers from scaling relationships can reduce the computational cost, although the application of these approaches has corresponding limitations. The common practices related to calculating and/or estimating coverage dependent TS energies are further discussed in the next section, along with the corresponding advantages, assumptions, and limitations. We note that in addition to affecting kinetics in a spectator role for an elementary step, in some cases, the accumulating surface species may participate directly in elementary steps through new bimolecular mechanisms, which can have even more profound effects by offering alternative, lower barrier, reaction pathways.[55,56] For example, on Ru surfaces that experience significant coverages of water during Fischer-Tropsch synthesis, the surface-bound water species enable hydrogen shuttling, ultimately influencing both rates and selectivities.[57] While important, the investigation of such direct roles of accumulating species in reaction chemistry is beyond the scope of this discussion.

2.3. Determining coverage-dependent reaction barriers

2.3.1. Scaling relationship approximations of coverage-dependent reaction barriers

A Brønsted-Evans-Polyani (BEP) relationship linearly relates the activation energy barriers and the reaction energies for a given elementary reaction or a family of reactions.[58] In general, as the thermodynamics of an elementary step become more favorable, the elementary step also becomes more kinetically favorable. The BEP relations are typically parametrized using a small set of DFT calculations, which are then used to estimate the barriers from thermodynamic values, thus significantly reducing computational costs in determining kinetic barriers.[8,29,53] Such scaling relations are widely used in the field and are effective for low-coverage MKM-based screening across catalyst compositions to identify catalysts with optimal binding properties while circumventing extensive TS searches.[1,5,12,13,59] However, the

applications of scaling relationships in high coverage environments are not yet well-established, including whether they can be universally applicable to diverse reactions and surfaces. Here, we introduce previous practices in utilizing a scaling relationship to estimate high-coverage barriers and discuss examples where scaling relationships may not be applicable.

In some cases, the BEP parameters (i.e., the slope and intercept of the linear relationship) derived at low-coverage conditions may also apply to the high coverage environment, such that one can apply the same BEP parameters to predict activation energies at high coverage conditions from high coverage reaction energies. Doing so avoids the need for conducting any computationally intensive high-coverage TS searches. Nørskov and Grabow utilized this approach[1,13] based on their observation that N_2 dissociation barriers on Ru with high spectator coverages (N* and O* at 0.5 ML) can be predicted by the BEP linear trend that was derived at low-coverage conditions across different metal surfaces (**Fig. 2a**).[60] Using low-coverage BEP parameters at high-coverage conditions relies upon the assumption that activation barriers and reaction energies scale across different coverages (on a single metal) in the same way that they scale across different metals (in a low-coverage environment). This assumption may be valid if the changes in reaction energies across surfaces and across coverages are caused by the same physical phenomenon (e.g., changes in the d-band center).[13]

Other effects, such as lateral through-space interactions between surface bound species, could also influence the energy of the TS and lead to high-coverage energetics that do not follow the low-coverage BEP relation. For example, Studt and coworkers used the scaling relationships derived at low-coverage conditions (0.25 ML CO*) across a suite of metals to predict TS energies at higher CO*-coverages for elementary steps involved in CO methanation.[12] In doing so, the authors observed that the energetics for a C-OH splitting step did not follow the BEP relation in the transition from low to high coverages,[12] hinting that a low-coverage BEP relation does not universally apply across coverages in all cases. Instead, Studt and coworkers derived new BEP parameters at a single, consistent high-coverage condition (1 ML CO*) across the suite of metal surfaces **(Fig. 2b)**.[12] Unlike the first approach, which circumvents the need for any high-coverage TS searches by using low-coverage BEP parameters, this approach does require a subset of high-coverage TS searches to parametrize the new BEP relation. Importantly, the outcome is a more accurate description of TS energies that do not scale universally across metals and coverages.

Alternatively, a coverage-dependent BEP relationship can be derived by calculating the reaction energy and activation barrier of an elementary step on a single surface at incremental coverages of a relevant spectator. For example, Schneider and coworkers explicitly calculated coverage-dependent activation barriers and reaction energies for O_2 dissociation on O*-covered Pt(111) (**Fig. 2c)**, where O* coverage varied between 0-0.5 ML. In this study, the authors enumerated the number of adsorbate-adsorbate interactions a species experiences at a given O*-coverage, and posited that the coverage-dependent O_2

dissociation correlation was linear because the number of interactions in the transition- and final-states was identical across coverages.[8]

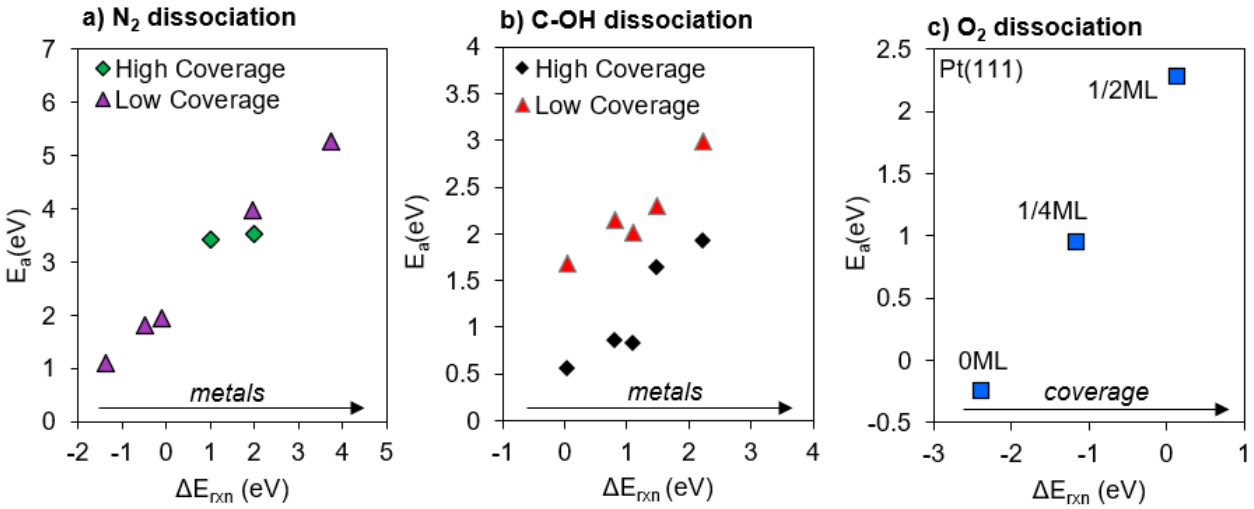

Figure 2. BEP relations between activation energies (E_a) and the reaction energies (ΔE_{rxn}) for **(a)** N_2 dissociation across close packed surfaces of different transition-metals (fcc(111), hcp(0001), and bcc(110)) at low coverage (purple triangles) and on Ru(0001) with 0.5 ML of O* and N* (green diamonds); **adapted with permission from**[60]. Copyright 2002 Elsevier. **(b)** C-OH dissociation with ¼ ML CO* (red triangles) and 1 ML CO* (black diamonds) spectators on the (211) surfaces of Ag, Cu, Pd, Pt, and Rh. All energies are relative to CO and H_2 in the gas phase. 1 ML coverage for the (211) surface is defined as one adsorbate per atom along the step; **adapted with permission from**[12]. Copyright 2013 Elsevier. **(c)** O_2 dissociation on O*-covered Pt(111) surfaces. All energies are taken relative to the energies of O_2(g) and Pt(111) surface; **adapted with permission from**[8]. Copyright 2010 Wiley-VCH.

Table 1. Reported activation barriers (E_a) and reaction energies (ΔE_{rxn}) of elementary steps on metal surfaces at low (no spectator species) and high (some spectator species) coverages.

Elementary Step	Surface[ref]	Spectator Species	Low Coverage		High Coverage	
			E_a (eV)	ΔE_{rxn} (eV)	E_a (eV)	ΔE_{rxn} (eV)
NOH* + H* → HNOH* + *	Pt(111)[9]	1/2 ML NO*	1.09	-0.02	1.24	-0.86
HNO* + H* → HNOH * + *			0.36	-0.15	0.43	-0.74
N* + N* → N_2* + *			1.55	-1.94	1.60	-2.28
CH_2OOH* → CH_2O* + OH*	Cu(211)[16]	1/6 ML HCOO*	0.42	0.35	0.49	0.34
OH* + OH* → H_2O* + O*	Pd(100)[27,a]	0.30 ML O* and 0.42 ML H*	0.24	0.21	1.34	-0.87
COOH* + * → CO_2* + H*	Pt(100)[15,a]	4/9 ML CO*	0.73	-0.1	0.96	-0.39
COOH* + * → CO_2* + H*			0.96	0.13	1.18	-0.01
CO* + O* → CO_2			0.75	0.01	0.79	-0.62
CHO* + H* → HCOH*+ *	Ru_{218}[61]	1 ML CO*	0.82	-0.26	0.75	0.12

[a] with free energy corrections

These prior reports demonstrate that the BEP relationship can be applied to high-coverage conditions for certain reactions. However, based on our review of prior works reporting computed reaction energies and activation barriers at low and high coverages, we found numerous examples of elementary steps that deviate from the expectation. Specifically, if the BEP relation is valid across coverages, an elementary step that becomes more endothermic (exothermic) due to coverage effects should have an increased (decreased) activation barrier. **Table 1** provides several exceptions to this general BEP trend, revealing that adsorbates and TSs do not necessarily experience coverage effects in the same way. For example, for the hydroxyl disproportionation reaction (OH* + OH* → H_2O* + O*), the reaction energy became more thermodynamically favorable on Pd(100) as the surface became populated with O* and H* spectators (ΔE_{rxn} decreased from 0.21 to -0.87 eV; **Table 1**); yet the activation barrier increased by nearly 1 eV, from 0.24 to 1.34 eV, in contrast with the BEP relation. We note that **Table 1** reports a representative set of examples and not an exhaustive list from prior reports. These exceptions at high coverage environments may be due to several variables, such as: i) the size and geometry of the TSs, which will experience different degrees of through-space interactions, and/or ii) the identity of the spectator species, which may impose attractive or repulsive interactions on different surface-bound species. Our review of prior reports also indicates that the type of catalyst model (i.e., flat periodic super cells vs. curved nanoparticle models) can impact such trends.[61,62] Further studies are thus needed to explore the applicability of linear scaling relationships at high coverages, including factors that lead to exceptions, for diverse chemistries and surfaces.

Alternative to deriving BEP relations explicitly from calculated energetics, the so-called weighing factor (ω) method instead defines the slope of the line based on a property indicative of the 'earliness' or 'lateness' of a TS. In this way, the chosen weighing factor is used to relate the activation energy barrier to the reaction energy at varying coverages:[5,29,37,53]

$$E_{a,f}(\theta_j) = E_{a,f} + \omega(\Delta E_{rxn}(\theta_j) - \Delta E_{rxn}) \quad (15)$$

Here, $E_{a,f}$ and ΔE_{rxn} are constant, coverage-independent values whereas $\Delta E_{rxn}(\theta_j)$ and $E_{a,f}(\theta_j)$ are the coverage-dependent reaction energy and activation barrier, respectively. For a given coverage θ_j, the change in the magnitude of ΔE_{rxn} due to coverage effects is calculated, and a portion of that change is distributed - according to the magnitude of ω - to $E_{a,f}$. The reverse barrier is then calculated from **Eqn. 5**.

Note that the important physical distinction between the weighing factor method and the empirical BEP relationship is that the slope of the line described by **Eqn. 15** is an independent parameter based on a property of an elementary step (i.e., the earliness/lateness of the involved TS). In contrast, using a BEP relationship to predict coverage-dependent activation barriers requires explicit calculations of coverage-dependent TS's to initially parametrize (i.e., quantify the slope of) the line. For an early TS that is initial-

state-like (i.e., ω = 0), $E_{a,f}$ remains fixed, and the required change in energy is implicitly applied to $E_{a,r}$ via **Eqn. 5**. For a late TS that is final-state-like, ω = 1, and the required change in energy is applied wholly to $E_{a,f}$. These two extremes present scenarios where case (i), described in **Section 2.2**, might be applicable, though incorporating ω provides a physical justification. For $0 < \omega < 1$, the change is distributed across both $E_{a,r}$ and $E_{a,f}$. Note that it is necessary to apply the constraints that all barriers (forward and reverse) are positive, as **Eqn. 15** may lead to unphysical negative barriers in some cases. An important implication of the weighing factor method is the underlying assumption that the earliness/lateness of a TS at low-coverage conditions remains the same at high-coverage conditions, which may be inappropriate if the reaction energy changes dramatically with coverage; the Hammond's postulate suggests that the TS becomes more product-like (late TS) as the reaction becomes more endothermic.[63,64] Another key challenge is that the predicted $E_{a,f}$ values are sensitive to the choice of a quantifiable property to calculate ω, which requires normalization against defined initial-state or final-state values. The weighing factor has previously been based on coverage-dependent variations in initial- and final-state adsorption energies[53]; alternatively, a quantifiable geometric property such as a normalized bond length could represent the degree of bond formation/dissociation of an elementary step, and consequently the position of the TS along the reaction coordinate. A consistent and uniform method for calculating ω is not yet defined in the field.

Importantly, a key application of MKMs is low-cost, high-throughput, descriptor-based catalyst screening;[5] as such, it is convenient to utilize scaling relationships for on-the-fly coverage-dependent activation barrier or TS energy predictions. However, the use of scaling relationships to predict kinetic parameters at high-coverage conditions relies upon the preservation of the BEP relation at high-coverage, which may not apply for all chemistries, including for example those listed in **Table 1**. We acknowledge that when comparing the relative performance of catalysts, uniform errors across catalysts may not alter predicted trends in activity or selectivity – i.e., the shape of the volcano plot. For example, Grabow and coworkers reported that coverage-dependent MKMs with TS energies described by scaling relationships and lattice-based kMC simulations, that explicitly consider spatial distributions of surface species, predicted the same trends across metals (reactivity, rate-limiting steps) for the CO oxidation reaction.[1] Still, further studies are needed to define the range of applicability of BEP relationships for predicting trends across materials or elucidating detailed reaction mechanisms on a single material in high-coverage catalytic systems.

2.3.2. First-principles calculations of coverage-dependent TS energies

Conducting explicit DFT calculations in the presence of spectator species (i.e., MASI(s)) is the most intensive method for determining coverage-dependent TS energies. This method attempts to determine the first principles-based energetics of TSs in the presence of spectator species, thereby accounting for lateral

interactions in both thermodynamic and kinetic parameters within the MKM. As discussed earlier, these calculations are necessary to generate a high coverage or coverage-dependent BEP relation distinct from the low-coverage BEP relation, as described in **Section 2.3.1**. The primary challenges of conducting these calculations arise in the nontrivial design of atomic-scale models for DFT calculations and the large number of permutations for different geometries of adsorbates. The number of calculations may be reduced by applying coverage-dependent TS searches to only a few kinetically relevant steps, if the identity of kinetically relevant step(s) is known. However, identifying these steps requires some knowledge of the model solutions, imposing a circular problem, as steps that are predicted to be kinetically relevant based on model solutions parameterized by low-coverage DFT calculations may differ from those parameterized by high-coverage DFT calculations. We also reiterate that mean-field model solutions cannot distinguish nor predict spatial adsorbate configurational effects on reaction rates. However, the configuration of adsorbates in atomic-scale models will affect the DFT-derived energetics used to parametrize a mean-field model through lateral interactions. Various strategies have been implemented in the literature to reduce the computational cost and the number of DFT calculations required to directly compute coverage dependent energetics, and these are briefly discussed here.

(a) Performing TS searches on size-reduced periodic unit cells

The size of the periodic unit cell is a key attribute of DFT surface simulations that impacts computational cost and is also directly related to surface coverage. Using a small unit cell reduces the cost of the DFT calculations, which are well-known to scale cubically with the number of electrons in the system. Yet, the use of smaller unit cell sizes also limits the granularity of a periodic model and increases the incremental surface concentration of all species. For example, consider a periodic slab model for which a 2×2 unit cell contains four exposed metal atoms (**Fig. 3**). Following convention, the unit cell is defined as having four possible active sites in microkinetic models, where a single adsorbate within the unit cell has a fractional coverage denoted as 1/4 ML. A 2×2 model can only capture 1/4 ML increments of coverage for an adsorbate that occupies a single site, in contrast with a larger 3×3 unit cell with nine surface atoms, that can capture smaller 1/9 ML increments. This difference may result in slightly different parameters for the fitted equations of coverage-dependent energies (i.e., **Eqn. 13**). Interestingly, Vlachos and coworkers compared calculated activation barriers for ethanol and ethylene glycol decomposition reactions on 2×2 and 3×3 surface slab models, and concluded that the different cell sizes had no statistically significant influence on BEP correlation parameters.[65]

Others have also used relatively small unit cells to calculate coverage-dependent TS energies for application in MKMs.[9,29] Yet, the possible site permutations of adsorbate configurations imposed by periodicity and exacerbated by use of a smaller unit cell may fail to capture physically relevant adsorbate

arrangements, which may be otherwise permitted on larger unit cells**.** For example, Hu and coworkers studied ordered CO* structures on Pt slab models and found that the periodic 4×4 unit cell could not capture the ordered (√3×√3)R30°-CO structure and, consequently, could not predict the coverage at which the preferred CO* adsorption site transitioned from bridge sites to top sites.[66] Ultimately, reducing unit cell sizes offers a convenient but not inconsequential method for performing computationally tractable high-coverage TS searches.

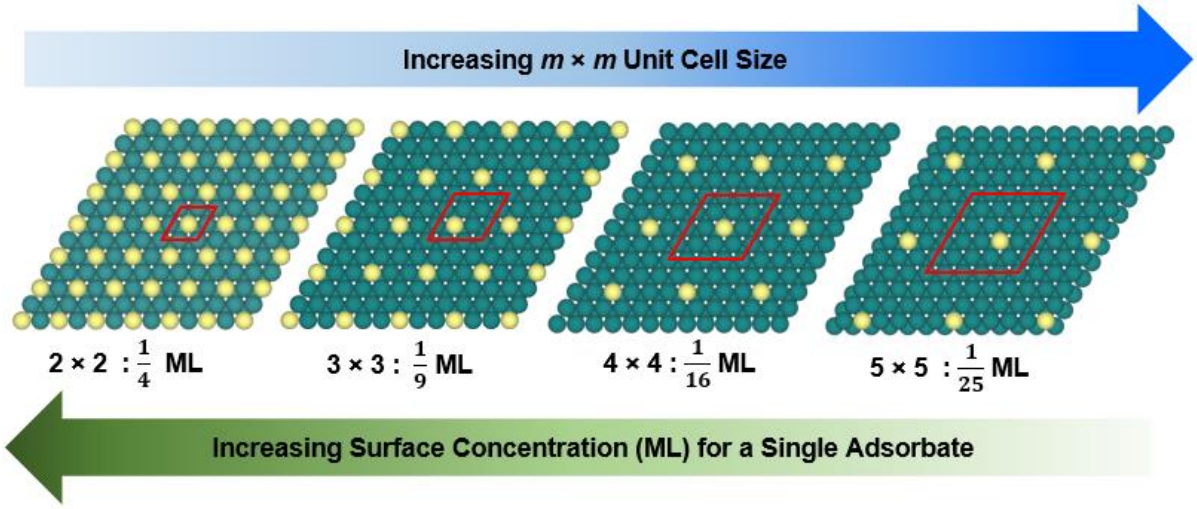

Figure 3. Relationship between unit cell size (red boxes) and the smallest increment of surface concentration (yellow) that can be simulated (monolayer, ML) for an *m x m* periodic slab model of a close-packed (0001) hcp metal surface facet.

(b) Calculating TS energies at incremental spectator coverages

As with coverage-dependent binding energies (**Eqn. 13**), TS energies can be calculated in the presence of different concentrations of spectator species, such that E_{TS} is described as a function of the surface coverage of an intermediate(s), and E_{TS} values are updated iteratively within the MKM simulation:

$$E_{TS} = f(\theta_j) \tag{16}$$

In **Eqn. 16**, the independent variable is the surface coverage of an intermediate *j*, whereas in a BEP relation the independent variable is a coverage-dependent reaction energy. In both formalisms, due to the computational cost, the mathematical equation (i.e., **Eqn. 16** or a BEP relation) is typically parametrized against a small set of DFT calculations (i.e., at few coverage increments). The discussion in this section focuses on the more general **Eqn. 16**, but we note that the challenges related to calculating TS energies at incremental coverages are relevant to parameterizing BEP relations as well. Yang and coworkers, for example, calculated the energies of TSs involved in methanol synthesis on Cu(211) surfaces in the presence of incremental equilibrated concentrations of bidentate formate spectators and reported the corresponding activation barriers, which can be used to generate **Eqn. 16**.[16] Representative activation barriers and TS

geometries from this study for the CO_2 hydrogenation (CO_2* + H* → COOH* + *) and CO_2 dissociation (CO_2* + * → CO* + O*) elementary steps are shown in **Figure 4**.

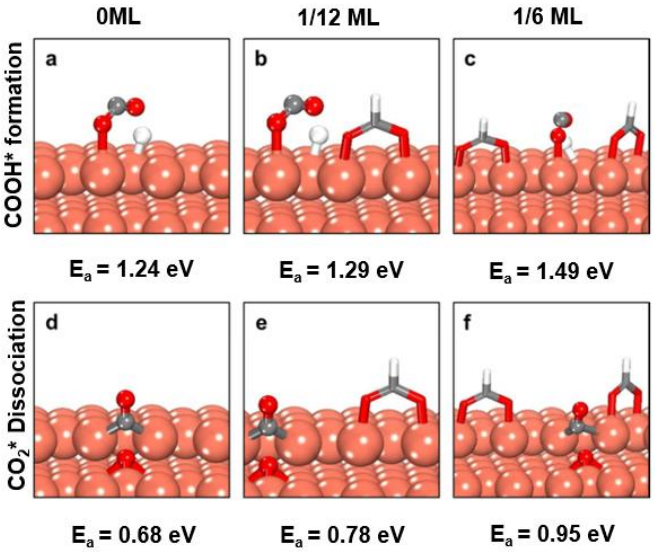

Figure 4. Optimized configurations and calculated activation barriers of **(a – c)** COOH formation and **(d – f)** CO_2 dissociation on **(a, d)** clean Cu(211) and Cu(211) with **(b, e)** 1/12 ML and **(c, f)** 1/6 ML pre-adsorbed formate. The spectating formate species are shown as sticks, while the reaction intermediates are presented as balls and sticks. **Reproduced from** [16]. Copyright 2017 American Chemical Society.

A significant component of the computational cost involved in determining the functional form of **Eqn. 16** lies in finding the most stable (equilibrated) arrangement of spectator species at each incremental coverage, as there are multiple atomic configurations congruent with a single surface concentration. Finding the minimum-energy configuration of spectator species for a given surface concentration typically requires first optimizing the model system for each spectator concentration (e.g., finding the local minima). The arrangement of spectator species at a given concentration is then defined as the lowest-energy configuration among all optimized configurations (e.g., the global minimum). This optimization process may be repeated for each species (adsorbate or transition-state), as different configurations of spectators will influence the stabilities of other bound intermediates. As an illustrative example, the effect of spectator configuration on the adsorption energy of an intermediate is demonstrated in **Figure 5**. A hydroxyl (OH*) group is adsorbed in the presence of two different configurations of 2/9 ML CO* on Ru(0001). Distinct CO* arrangements, even at a single concentration, result in OH* adsorption energies that differ by >10 kJ mol^{-1}. These differences would ultimately impact the energies and geometries of elementary steps that involve OH* in the initial-, final-, or transition states. We note that the effects of different spectator concentrations are expected to be more significant for larger adsorbates that occupy more than one site (e.g., bidentate formate) or at higher coverages of spectator species, where lateral interactions would be enhanced.

Incremental coverage calculations provide the form and parameters for **Eqn. 16.** Because generating the numerous permutations is a computationally intensive task, automating the process is ideal.[15,67] Once interactions among adsorbates (e.g., the first and second neighbors) and adsorbate-surface are established, these datasets can also be used to parametrize cluster expansions (CEs), which describe lateral interactions among adsorbates by expanding the energy of a configuration into *n*-body interaction terms; the resulting expression is capable of predicting energies of any given configuration of adsorbates.[4,33] When applied to TSs,[68,69] this method generates an expression analogous to **Eqn. 16.** Machine-learning (ML) approaches have also been utilized to parametrize CEs or directly predict activation barriers at high coverage.[70,71] Ultimately, determining **Eqn. 16** or CEs through rigorous, coverage-dependent TS calculations can be a computationally tractable option for simple reaction networks composed of small intermediates and few elementary steps.

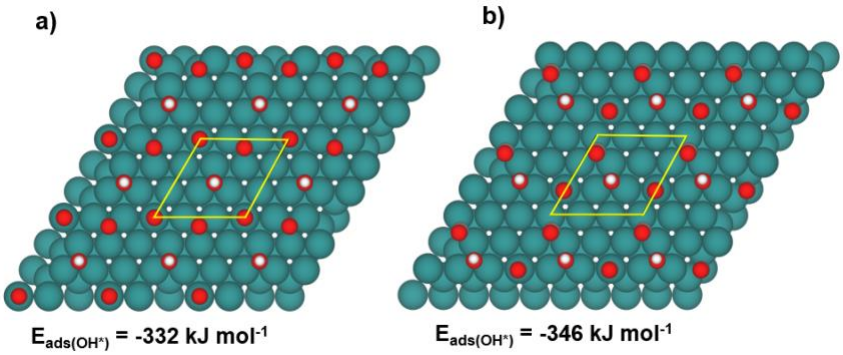

Figure 5. Top-view snapshots of OH* adsorbed on two different configurations (a, b) of 2/9 ML CO* spectators on 3 × 3 Ru(0001) periodic unit cells and the average OH* adsorption energy of the system.

(c) Calculating TS energies with fixed spectator configurations

If parametrizing **Eqn. 16** is computationally intractable, one possible simplification is to fix the adsorption site of the spectator species in the presence of the reaction intermediates or TSs. This removes the need to perform large numbers of calculations to search for the minimum-energy configuration of adsorbates at a given concentration of spectator species and can be motivated by some knowledge of adsorbate distributions provided by experiments (e.g., low energy electron diffraction (LEED) or scanning tunneling microscopy (STM)). For example, Schneider and coworkers used this approach to model reaction intermediates in the presence of spectator O* species on Pt(111) surfaces. The O*-atom locations were based on O*-coverage patterns derived from prior Monte Carlo simulations in corroboration with STM performed under O_2 environments on Pt(111).[72] We note that this simplification may fail to capture the global minima if the configuration (i.e., geometry or binding site) of spectator species changes as the

intermediates and TSs are introduced to the system.[14] As such, the effects of this assumption on calculated energetics can be variable and difficult to determine a priori.

(d) Calculating TS energies at a single representative spectator coverage

A commonly utilized simplification to parametrizing **Eqn. 16** or a high-coverage BEP relation is to simulate a single, representative surface concentration of spectator species to generate a set of high-coverage energetic parameters (i.e., values at a defined coverage rather than coverage dependent equations). The appropriate concentration can be informed by the low-coverage, steady-state MKM predicted MASI coverage or experimental kinetic and/or spectroscopic data. In this case, the calculated, high-coverage TS energies are fixed parameters in the MKM, under the assumption that the spectator coverage employed in the DFT calculations will be similar to the high-coverage, steady-state solution (i.e., coverage self-consistent MKM). Mavrikakis and coworkers used this approach to describe coverage-dependent TS energies in a mean-field MKM describing formic acid decomposition, yielding TOFs, apparent activation energies, and apparent reaction orders in good parity with companion experiments.[14] However, we note that utilizing a single, representative surface coverage for model parameterization limits the MKM to describing the range of conditions relevant to the chosen coverage and lacks the granularity in the coverage-dependent energetic parameters afforded by **Eqn. 16.**

(e) Adapting low-coverage TS geometries to high-coverage systems

The computational complexity of conducting TS-searches in the presence of spectator species can be reduced by utilizing TS structures derived at the clean-surface limit (i.e., low coverage) as initial guesses for high-coverage TS optimization. Hu and coworkers utilized this method to determine TS energies in the presence of CO* spectators by optimizing the TS geometries at low-coverage conditions, fixing the resulting geometries, and generating permutations of TS and CO*-spectator arrangements at incremental concentrations.[73] Once the global minimum configuration was found for a given spectator concentration, the authors performed a final refinement of the TS geometry in the presence of the CO* spectators via the constrained optimization scheme. This strategy circumvents the need for TS searches at incremental spectator concentrations, reducing the computational cost and complexity, but does not allow for consideration of more extensive effects of coadsorbates on the structure of the TS.

3. Conclusions and future outlook

Mean-field MKMs parameterized with DFT-derived energetics provide a powerful tool for determining reaction mechanisms, identifying key properties dictating catalyst performance, and screening

the vast space of catalytic materials for a targeted reaction. The field has made substantial progress towards defining best practices in describing coverage-dependent adsorption energies in MKMs,[8,13,25,38,39] facilitating predictions of adsorbate quantities that are critical in predicting accurate turnovers. In this perspective, we expand on recent work in the field aimed at coverage-dependent descriptions of *thermodynamic* parameters by providing a systematic assessment of approaches for calculating and implementing coverage-dependent *kinetic* parameters within MKMs.

Coverage-dependent thermodynamic (adsorption and reaction energies) and kinetic (activation barriers) parameters are inherently correlated within the MKM codes. Decoupling these values can lead to physically unrealistic solutions. Several strategies implemented in the literature capture some degree of coverage effects on kinetic parameters while conserving computational cost. BEP relationships, which have been successfully applied in low-coverage MKM-based catalyst screening, can reduce the computational costs in explicitly calculating TS energies, by predicting coverage-dependent E_{TS} (or $E_{a,f}$) based on coverage-dependent reaction energies. While there are several cases reported in the literature where the low-coverage BEP relations remain valid at high-coverage, several general exceptions to the universality of the BEP relation at high coverage environments are also identified. That is, when an elementary step that becomes more endothermic (exothermic) due to coverage effects does not exhibit the expected increased (decreased) activation barrier. Thus, whereas linear scaling relationships offer a convenient method for predicting coverage-dependent kinetics, there is a clear need for targeted studies exploring the applicability of BEP relationships at high coverages, including factors that lead to exceptions, for varied chemistries and surfaces.

When linear scaling relationships are not applicable or known, it becomes necessary to conduct high-coverage TS searches for elementary steps. Various simplifications have been applied to execute such calculations using periodic surface models with a reasonable computational cost. These simplifications, while necessary for practical computational tractability, do imply restrictions on certain quantities and/or configurations of adsorbates and transition states. Thus, several practical questions remain about the physical relevance of these assumptions and the effect on the resulting high-coverage TS energy, and corresponding MKM predictions, for diverse systems. We note that most published reports of high-coverage TS calculations involve systems with relatively small, single-site spectator species (CO*, O*, NO*),[8,9,14,54] with bidentate formate representing one of the largest spectators evaluated;[16] describing systems with larger MASIs will require approaches that reduce the computational cost relative to those currently available. Recent advances in the field have utilized ML methods to predict coverage-dependent adsorption and/or TS energies, or to parametrize cluster expansions that describe high-coverage energies.[70,71] Further development of these predictive models will play a key role in reducing the total number of calculations necessary to describe high-coverage kinetic parameters, thereby enabling more

facile construction of coverage-dependent MKMs for larger reaction networks and reacting species. Yet, ML approaches also rely on DFT-derived training data, further highlighting the need to establish physically relevant methodologies for high-coverage TS searches in atomistic models.

Challenges in establishing effective approaches for integrating coverage-dependent kinetic parameters in MKMs are exacerbated by sporadically documented methods describing the approach used to estimate high-coverage TS energies and incorporate coverage-dependent kinetics into MKMs, and the lack of direct benchmarking of MKM kinetic parameters. It is inferred that small changes in DFT-derived parameters will lead to dramatic changes in MKM solutions, based on the exponential nature of rate and equilibrium constants. We note that MKMs are often validated against macroscale steady-state kinetic data (e.g., TOFs, E_{app}, reaction orders),[15,29,54,67,74] despite the possibility that multiple solutions can lead to steady-state predictions in good parity with experiments. Thus, while prior reports have notably documented the improved accuracy of models (TOFs, selectivities) upon the incorporation of coverage-dependent kinetic and thermodynamic parameters for specific reaction systems,[15,27,28,53] there remains a gap in understanding the accuracy of and errors associated with coverage-dependent kinetic parameters at the elementary step level and validation of the methods used for varying systems. To address this gap, there is a need for experimental data that would allow for benchmarking of elementary step energetics computed at high coverage alongside investigations focused specifically on establishing best-practices for estimating and incorporating coverage-dependent kinetics in MKMs. This further research will be instrumental to advancing the utility of MKMs in heterogeneous catalyst development in increasingly complex reaction environments, such as those found in diverse chemistries important for mitigating greenhouse gas emissions and decarbonizing the energy and chemical sectors.

Acknowledgements

This work was authored in part by the National Renewable Energy Laboratory, operated by Alliance for Sustainable Energy, LLC, for the U.S. Department of Energy (DOE) under Contract No. DE-AC36-08GO28308. Funding provided by the U.S. Department of Energy Office of Energy Efficiency and Renewable Energy Bioenergy Technologies Office. The views expressed in the article do not necessarily represent the views of the DOE or the U.S. Government. The U.S. Government retains and the publisher, by accepting the article for publication, acknowledges that the U.S. Government retains a nonexclusive, paid-up, irrevocable, worldwide license to publish or reproduce the published form of this work, or allow others to do so, for U.S. Government purposes. A portion of the research was performed using computational resources sponsored by the Department of Energy's Office of Energy Efficiency and Renewable Energy and located at the National Renewable Energy Laboratory. M.N. thanks the Mines

VPRTT Materials Science Graduate Fellowship Program funded by the National Science Foundation award (OAC 2118201).

References

(1) Li, X.; Grabow, L. C. Evaluating the Benefits of Kinetic Monte Carlo and Microkinetic Modeling for Catalyst Design Studies in the Presence of Lateral Interactions. *Catal. Today* **2022**, *387*, 150–158. https://doi.org/10.1016/j.cattod.2021.03.010.
(2) Motagamwala, A. H.; Dumesic, J. A. Microkinetic Modeling: A Tool for Rational Catalyst Design. *Chem. Rev.* **2021**, *121* (2), 1049–1076. https://doi.org/10.1021/acs.chemrev.0c00394.
(3) Chen, B. W. J.; Xu, L.; Mavrikakis, M. Computational Methods in Heterogeneous Catalysis. *Chem. Rev.* **2021**, *121* (2), 1007–1048. https://doi.org/10.1021/acs.chemrev.0c01060.
(4) Matera, S.; Schneider, W. F.; Heyden, A.; Savara, A. Progress in Accurate Chemical Kinetic Modeling, Simulations, and Parameter Estimation for Heterogeneous Catalysis. *ACS Catal.* **2019**, *9* (8), 6624–6647. https://doi.org/10.1021/acscatal.9b01234.
(5) Grabow, L. C. Computational Catalyst Screening. In *Computational Catalysis*; Asthagiri, A., Janik, M. J., Eds.; The Royal Society of Chemistry, 2013; pp 1–58. https://doi.org/10.1039/9781849734905-00001.
(6) Filot, I. A. W. *Introduction to Microkinetic Modeling*; Eindhoven University of Technology, 2018.
(7) Aarons, J.; Sarwar, M.; Thompsett, D.; Skylaris, C.-K. Perspective: Methods for Large-Scale Density Functional Calculations on Metallic Systems. *J. Chem. Phys.* **2016**, *145* (22), 220901. https://doi.org/10.1063/1.4972007.
(8) Getman, R. B.; Schneider, W. F. DFT-Based Coverage-Dependent Model of Pt-Catalyzed NO Oxidation. *ChemCatChem* **2010**, *2* (11), 1450–1460. https://doi.org/10.1002/cctc.201000146.
(9) Farberow, C. A.; Dumesic, J. A.; Mavrikakis, M. Density Functional Theory Calculations and Analysis of Reaction Pathways for Reduction of Nitric Oxide by Hydrogen on Pt(111). *ACS Catal.* **2014**, *4* (10), 3307–3319. https://doi.org/10.1021/cs500668k.
(10) Loveless, B. T.; Buda, C.; Neurock, M.; Iglesia, E. CO Chemisorption and Dissociation at High Coverages during CO Hydrogenation on Ru Catalysts. *J. Am. Chem. Soc.* **2013**, *135* (16), 6107–6121. https://doi.org/10.1021/ja311848e.
(11) Allian, A. D.; Takanabe, K.; Fujdala, K. L.; Hao, X.; Truex, T. J.; Cai, J.; Buda, C.; Neurock, M.; Iglesia, E. Chemisorption of CO and Mechanism of CO Oxidation on Supported Platinum Nanoclusters. *J. Am. Chem. Soc.* **2011**, *133* (12), 4498–4517. https://doi.org/10.1021/ja110073u.
(12) Lausche, A. C.; Medford, A. J.; Khan, T. S.; Xu, Y.; Bligaard, T.; Abild-Pedersen, F.; Nørskov, J. K.; Studt, F. On the Effect of Coverage-Dependent Adsorbate–Adsorbate Interactions for CO Methanation on Transition Metal Surfaces. *J. Catal.* **2013**, *307*, 275–282. https://doi.org/10.1016/j.jcat.2013.08.002.
(13) Grabow, L. C.; Hvolbæk, B.; Nørskov, J. K. Understanding Trends in Catalytic Activity: The Effect of Adsorbate–Adsorbate Interactions for CO Oxidation Over Transition Metals. *Top. Catal.* **2010**, *53* (5–6), 298–310. https://doi.org/10.1007/s11244-010-9455-2.

(14) Li, S.; Rangarajan, S.; Scaranto, J.; Mavrikakis, M. On the Structure Sensitivity of and CO Coverage Effects on Formic Acid Decomposition on Pd Surfaces. *Surf. Sci.* **2021**, *709*, 121846. https://doi.org/10.1016/j.susc.2021.121846.
(15) Bhandari, S.; Rangarajan, S.; Maravelias, C. T.; Dumesic, J. A.; Mavrikakis, M. Reaction Mechanism of Vapor-Phase Formic Acid Decomposition over Platinum Catalysts: DFT, Reaction Kinetics Experiments, and Microkinetic Modeling. *ACS Catal.* **2020**, *10* (7), 4112–4126. https://doi.org/10.1021/acscatal.9b05424.
(16) Wu, P.; Yang, B. Significance of Surface Formate Coverage on the Reaction Kinetics of Methanol Synthesis from CO_2 Hydrogenation over Cu. *ACS Catal.* **2017**, *7* (10), 7187–7195. https://doi.org/10.1021/acscatal.7b01910.
(17) Chen, Z.; Liu, Z.; Xu, X. XPK: Toward Accurate and Efficient Microkinetic Modeling in Heterogeneous Catalysis. *ACS Catal.* **2023**, *13* (23), 15219–15229. https://doi.org/10.1021/acscatal.3c04298.
(18) Razdan, N. K.; Bhan, A. Kinetic Description of Site Ensembles on Catalytic Surfaces. *Proc. Natl. Acad. Sci. U.S.A.* **2021**, *118* (8), e2019055118. https://doi.org/10.1073/pnas.2019055118.
(19) Ge, J.; Adams, K. C.; Peters, B. Microkinetic Models with Interacting Adsorbates and Langmuir–Hinshelwood Steps: Solving the Master Equation on Small Periodic Tiles. *J. Phys. Chem. C* **2023**, acs.jpcc.3c07387. https://doi.org/10.1021/acs.jpcc.3c07387.
(20) Pineda, M.; Stamatakis, M. Beyond Mean-Field Approximations for Accurate and Computationally Efficient Models of on-Lattice Chemical Kinetics. *J. Chem. Phys.* **2017**, *147* (2), 024105. https://doi.org/10.1063/1.4991690.
(21) Goswami, A.; Schneider, W. F. Mean Field Model Parameterization to Recover Coverage-Dependent Kinetics. *J. Catal.* **2023**, *426*, 352–360. https://doi.org/10.1016/j.jcat.2023.07.013.
(22) Razdan, N. K.; Bhan, A. Catalytic Site Ensembles: A Context to Reexamine the Langmuir-Hinshelwood Kinetic Description. *Journal of Catalysis* **2021**, *404*, 726–744. https://doi.org/10.1016/j.jcat.2021.09.016.
(23) Hellman, A.; Honkala, K. Including Lateral Interactions into Microkinetic Models of Catalytic Reactions. *The Journal of Chemical Physics* **2007**, *127* (19), 194704. https://doi.org/10.1063/1.2790885.
(24) Hansen, E. W.; Neurock, M. First-Principles-Based Monte Carlo Simulation of Ethylene Hydrogenation Kinetics on Pd. *Journal of Catalysis* **2000**, *196* (2), 241–252. https://doi.org/10.1006/jcat.2000.3018.
(25) Bajpai, A.; Frey, K.; Schneider, W. F. Comparison of Coverage-Dependent Binding Energy Models for Mean-Field Microkinetic Rate Predictions. *Langmuir* **2020**, *36* (1), 465–474. https://doi.org/10.1021/acs.langmuir.9b03563.
(26) Xie, W.; Xu, J.; Chen, J.; Wang, H.; Hu, P. Achieving Theory–Experiment Parity for Activity and Selectivity in Heterogeneous Catalysis Using Microkinetic Modeling. *Acc. Chem. Res.* **2022**, *55* (9), 1237–1248. https://doi.org/10.1021/acs.accounts.2c00058.
(27) Zhao, J.; Yao, Z.; Bunting, R. J.; Hu, P.; Wang, J. Microkinetic Modeling with Size-Dependent and Adsorbate–Adsorbate Interactions for the Direct Synthesis of H_2O_2 over Pd Nanoparticles. *ACS Catal.* **2023**, *13* (22), 15054–15073. https://doi.org/10.1021/acscatal.3c03893.
(28) Yao, Z.; Zhao, J.; Bunting, R. J.; Zhao, C.; Hu, P.; Wang, J. Quantitative Insights into the Reaction Mechanism for the Direct Synthesis of H_2O_2 over Transition Metals: Coverage-

Dependent Microkinetic Modeling. *ACS Catal.* **2021**, *11* (3), 1202–1221. https://doi.org/10.1021/acscatal.0c04125.
(29) Grabow, L. C.; Gokhale, A. A.; Evans, S. T.; Dumesic, J. A.; Mavrikakis, M. Mechanism of the Water Gas Shift Reaction on Pt: First Principles, Experiments, and Microkinetic Modeling. *J. Phys. Chem. C* **2008**, *112* (12), 4608–4617. https://doi.org/10.1021/jp7099702.
(30) Chen, Z.; Liu, Z.; Xu, X. Coverage-Dependent Microkinetics in Heterogeneous Catalysis Powered by the Maximum Rate Analysis. *ACS Catal.* **2021**, *11* (15), 9333–9344. https://doi.org/10.1021/acscatal.1c01997.
(31) Yang, Y.; Shen, T.; Xu, X. Understanding the Source of Error in First-Principles-Based Micro-Kinetic Modeling: Density Functional Theory Calculations Versus the Mean-Field Approximation. *J. Phys. Chem. C* **2023**, *127* (20), 9631–9639. https://doi.org/10.1021/acs.jpcc.3c01710.
(32) Goswami, A.; Ma, H.; Schneider, W. F. Consequences of Adsorbate-Adsorbate Interactions for Apparent Kinetics of Surface Catalytic Reactions. *J. Catal.* **2022**, *405*, 410–418. https://doi.org/10.1016/j.jcat.2021.12.005.
(33) Frey, K.; Schmidt, D. J.; Wolverton, C.; Schneider, W. F. Implications of Coverage-Dependent O Adsorption for Catalytic NO Oxidation on the Late Transition Metals. *Catal. Sci. Technol.* **2014**, *4* (12), 4356–4365. https://doi.org/10.1039/C4CY00763H.
(34) Qi, L.; Li, J. Adsorbate Interactions on Surface Lead to a Flattened Sabatier Volcano Plot in Reduction of Oxygen. *J. Catal.* **2012**, *295*, 59–69. https://doi.org/10.1016/j.jcat.2012.07.019.
(35) Jaraíz, M.; Rubio, J. E.; Enríquez, L.; Pinacho, R.; López-Pérez, J. L.; Lesarri, A. An Efficient Microkinetic Modeling Protocol: Start with Only the Dominant Mechanisms, Adjust All Parameters, and Build the Complete Model Incrementally. *ACS Catal.* **2019**, *9* (6), 4804–4809. https://doi.org/10.1021/acscatal.9b00522.
(36) Bhandari, S.; Rangarajan, S.; Mavrikakis, M. Combining Computational Modeling with Reaction Kinetics Experiments for Elucidating the *In Situ* Nature of the Active Site in Catalysis. *Acc. Chem. Res.* **2020**, *53* (9), 1893–1904. https://doi.org/10.1021/acs.accounts.0c00340.
(37) Medford, A. J.; Shi, C.; Hoffmann, M. J.; Lausche, A. C.; Fitzgibbon, S. R.; Bligaard, T.; Nørskov, J. K. CatMAP: A Software Package for Descriptor-Based Microkinetic Mapping of Catalytic Trends. *Catal. Lett.* **2015**, *145* (3), 794–807. https://doi.org/10.1007/s10562-015-1495-6.
(38) Zhdanov, V. P. The Effect of Adsorbate-Induced Surface Reconstruction on the Apparent Arrhenius Parameters for Desorption. *Prog. Surf. Sci.* **1990**, *35* (1–4), 143–157. https://doi.org/10.1016/0079-6816(90)90032-F.
(39) Dietze, E. M.; Grönbeck, H. Ensemble Effects in Adsorbate–Adsorbate Interactions in Microkinetic Modeling. *J. Chem. Theory Comput.* **2023**, *19* (3), 1044–1049. https://doi.org/10.1021/acs.jctc.2c01005.
(40) McQuarrie, D. A. *Statistical Mechanics*; Harper & Row: New Yo.
(41) Eyring, H. The Activated Complex in Chemical Reactions. *The Journal of Chemical Physics* **1935**, *3* (2), 107–115. https://doi.org/10.1063/1.1749604.
(42) Doyle, P. J.; Savara, A.; Raiman, S. S. Extracting Meaningful Standard Enthalpies and Entropies of Activation for Surface Reactions from Kinetic Rates. *Reac Kinet Mech Cat* **2020**, *129* (2), 551–581. https://doi.org/10.1007/s11144-020-01747-2.

(43) Campbell, C. T.; Sprowl, L. H.; Árnadóttir, L. Equilibrium Constants and Rate Constants for Adsorbates: Two-Dimensional (2D) Ideal Gas, 2D Ideal Lattice Gas, and Ideal Hindered Translator Models. *J. Phys. Chem. C* **2016**, *120* (19), 10283–10297. https://doi.org/10.1021/acs.jpcc.6b00975.
(44) Savara, A. Standard States for Adsorption on Solid Surfaces: 2D Gases, Surface Liquids, and Langmuir Adsorbates. *J. Phys. Chem. C* **2013**, *117* (30), 15710–15715. https://doi.org/10.1021/jp404398z.
(45) Chen, B. W. J.; Mavrikakis, M. How Coverage Influences Thermodynamic and Kinetic Isotope Effects for H_2/D_2 Dissociative Adsorption on Transition Metals. *Catal. Sci. Technol.* **2020**, *10* (3), 671–689. https://doi.org/10.1039/C9CY02338K.
(46) Omoniyi, A.; Hensley, A. J. R. Coverage- and Facet-Dependent Multiscale Modeling of O* and H* Adsorption on Pt Catalytic Nanoparticles. *J. Phys. Chem. C* **2024**, *128* (17), 7073–7086. https://doi.org/10.1021/acs.jpcc.3c08335.
(47) Han, T.; Lee, I.; Cao, Y.; Zhou, X.; Zaera, F. Thermodynamics of Carbon Monoxide Adsorption on Cu/SBA-15 Catalysts: Under Vacuum versus under Atmospheric Pressures. *J. Phys. Chem. C* **2022**, *126* (6), 3078–3086. https://doi.org/10.1021/acs.jpcc.1c10722.
(48) Scott, A. P.; Radom, L. Harmonic Vibrational Frequencies: An Evaluation of Hartree−Fock, Møller−Plesset, Quadratic Configuration Interaction, Density Functional Theory, and Semiempirical Scale Factors. *J. Phys. Chem.* **1996**, *100* (41), 16502–16513. https://doi.org/10.1021/jp960976r.
(49) Streibel, V.; Aljama, H. A.; Yang, A.-C.; Choksi, T. S.; Sánchez-Carrera, R. S.; Schäfer, A.; Li, Y.; Cargnello, M.; Abild-Pedersen, F. Microkinetic Modeling of Propene Combustion on a Stepped, Metallic Palladium Surface and the Importance of Oxygen Coverage. *ACS Catal.* **2022**, *12* (3), 1742–1757. https://doi.org/10.1021/acscatal.1c03699.
(50) Christiansen, M. A.; Mpourmpakis, G.; Vlachos, D. G. DFT-Driven Multi-Site Microkinetic Modeling of Ethanol Conversion to Ethylene and Diethyl Ether on γ-Al2O3(1 1 1). *Journal of Catalysis* **2015**, *323*, 121–131. https://doi.org/10.1016/j.jcat.2014.12.024.
(51) Madon, R. J.; Braden, D.; Kandoi, S.; Nagel, P.; Mavrikakis, M.; Dumesic, J. A. Microkinetic Analysis and Mechanism of the Water Gas Shift Reaction over Copper Catalysts. *Journal of Catalysis* **2011**, *281* (1), 1–11. https://doi.org/10.1016/j.jcat.2011.03.008.
(52) Chen, J.; Jia, M.; Mao, Y.; Hu, P.; Wang, H. Diffusion Coupling Kinetics in Multisite Catalysis: A Microkinetic Framework. *ACS Catal.* **2023**, *13* (5), 2937–2947. https://doi.org/10.1021/acscatal.2c06026.
(53) Ding, Y.; Xu, Y.; Song, Y.; Guo, C.; Hu, P. Quantitative Studies of the Coverage Effects on Microkinetic Simulations for NO Oxidation on Pt(111). *J. Phys. Chem. C* **2019**, *123* (45), 27594–27602. https://doi.org/10.1021/acs.jpcc.9b08208.
(54) Deimel, M.; Prats, H.; Seibt, M.; Reuter, K.; Andersen, M. Selectivity Trends and Role of Adsorbate–Adsorbate Interactions in CO Hydrogenation on Rhodium Catalysts. *ACS Catal.* **2022**, *12* (13), 7907–7917. https://doi.org/10.1021/acscatal.2c02353.
(55) Lin, T. C.; De La Torre, U.; Hejazi, A.; Kwon, S.; Iglesia, E. Unimolecular and Bimolecular Formic Acid Decomposition Routes on Dispersed Cu Nanoparticles. *J. Catal.* **2021**, *404*, 814–831. https://doi.org/10.1016/j.jcat.2021.08.049.
(56) Hibbitts, D.; Iglesia, E. Prevalence of Bimolecular Routes in the Activation of Diatomic Molecules with Strong Chemical Bonds (O_2 , NO, CO, N_2) on Catalytic Surfaces. *Acc. Chem. Res.* **2015**, *48* (5), 1254–1262. https://doi.org/10.1021/acs.accounts.5b00063.

(57) Hibbitts, D. D.; Loveless, B. T.; Neurock, M.; Iglesia, E. Mechanistic Role of Water on the Rate and Selectivity of Fischer–Tropsch Synthesis on Ruthenium Catalysts. *Angew. Chem. Int. Ed.* **2013**, *52* (47), 12273–12278. https://doi.org/10.1002/anie.201304610.
(58) Van Santen, R. A.; Neurock, M.; Shetty, S. G. Reactivity Theory of Transition-Metal Surfaces: A Brønsted−Evans−Polanyi Linear Activation Energy−Free-Energy Analysis. *Chem. Rev.* **2010**, *110* (4), 2005–2048. https://doi.org/10.1021/cr9001808.
(59) Wang, S.; Temel, B.; Shen, J.; Jones, G.; Grabow, L. C.; Studt, F.; Bligaard, T.; Abild-Pedersen, F.; Christensen, C. H.; Nørskov, J. K. Universal Brønsted-Evans-Polanyi Relations for C–C, C–O, C–N, N–O, N–N, and O–O Dissociation Reactions. *Catal. Lett.* **2011**, *141* (3), 370–373. https://doi.org/10.1007/s10562-010-0477-y.
(60) Nørskov, J. K.; Bligaard, T.; Logadottir, A.; Bahn, S.; Hansen, L. B.; Bollinger, M.; Bengaard, H.; Hammer, B.; Sljivancanin, Z.; Mavrikakis, M.; Xu, Y.; Dahl, S.; Jacobsen, C. J. H. Universality in Heterogeneous Catalysis. *J. Catal.* **2002**, *209* (2), 275–278. https://doi.org/10.1006/jcat.2002.3615.
(61) Liu, J.; Hibbitts, D.; Iglesia, E. Dense CO Adlayers as Enablers of CO Hydrogenation Turnovers on Ru Surfaces. *J. Am. Chem. Soc.* **2017**, *139* (34), 11789–11802. https://doi.org/10.1021/jacs.7b04606.
(62) Vyas, M.; Fajardo-Rojas, F.; Gómez-Gualdrón, D. A.; Kwon, S. Theoretical Assessments of Pd–PdO Phase Transformation and Its Impacts on H_2O_2 Synthesis and Decomposition Pathways. *Catal. Sci. Technol.* **2023**, *13* (13), 3828–3848. https://doi.org/10.1039/D3CY00404J.
(63) Hammond, G. S. A Correlation of Reaction Rates. *J. Am. Chem. Soc.* **1955**, *77* (2), 334–338. https://doi.org/10.1021/ja01607a027.
(64) Kwon, S.; Deshlahra, P.; Iglesia, E. Reactivity and Selectivity Descriptors of Dioxygen Activation Routes on Metal Oxides. *Journal of Catalysis* **2019**, *377*, 692–710. https://doi.org/10.1016/j.jcat.2019.07.048.
(65) Sutton, J. E.; Vlachos, D. G. A Theoretical and Computational Analysis of Linear Free Energy Relations for the Estimation of Activation Energies. *ACS Catal.* **2012**, *2* (8), 1624–1634. https://doi.org/10.1021/cs3003269.
(66) Gunasooriya, G. T. K. K.; Saeys, M. CO Adsorption on Pt(111): From Isolated Molecules to Ordered High-Coverage Structures. *ACS Catal.* **2018**, *8* (11), 10225–10233. https://doi.org/10.1021/acscatal.8b02371.
(67) Chen, B. W. J.; Bhandari, S.; Mavrikakis, M. Role of Hydrogen-Bonded Bimolecular Formic Acid–Formate Complexes for Formic Acid Decomposition on Copper: A Combined First-Principles and Microkinetic Modeling Study. *ACS Catal.* **2021**, *11* (7), 4349–4361. https://doi.org/10.1021/acscatal.0c05695.
(68) Rehman, T.; Jaipal, M.; Chatterjee, A. A Cluster Expansion Model for Predicting Activation Barrier of Atomic Processes. *J. Comput. Phys.* **2013**, *243*, 244–259. https://doi.org/10.1016/j.jcp.2013.03.005.
(69) Verma, S.; Rehman, T.; Chatterjee, A. A Cluster Expansion Model for Rate Constants of Surface Diffusion Processes on Ag, Al, Cu, Ni, Pd and Pt(100) Surfaces. *Surf. Sci.* **2013**, *613*, 114–125. https://doi.org/10.1016/j.susc.2013.03.022.
(70) Mou, T.; Han, X.; Zhu, H.; Xin, H. Machine Learning of Lateral Adsorbate Interactions in Surface Reaction Kinetics. *Curr. Opin. Chem. Eng.* **2022**, *36*, 100825. https://doi.org/10.1016/j.coche.2022.100825.

(71) Tian, H.; Rangarajan, S. Machine-Learned Corrections to Mean-Field Microkinetic Models at the Fast Diffusion Limit. *J. Phys. Chem. C* **2021**, *125* (37), 20275–20285. https://doi.org/10.1021/acs.jpcc.1c04495.
(72) Smeltz, A. D.; Getman, R. B.; Schneider, W. F.; Ribeiro, F. H. Coupled Theoretical and Experimental Analysis of Surface Coverage Effects in Pt-Catalyzed NO and O_2 Reaction to NO_2 on Pt(111). *Catal. Today* **2008**, *136* (1–2), 84–92. https://doi.org/10.1016/j.cattod.2007.12.139.
(73) Yao, Z.; Guo, C.; Mao, Y.; Hu, P. Quantitative Determination of C–C Coupling Mechanisms and Detailed Analyses on the Activity and Selectivity for Fischer–Tropsch Synthesis on Co(0001): Microkinetic Modeling with Coverage Effects. *ACS Catal.* **2019**, *9* (7), 5957–5973. https://doi.org/10.1021/acscatal.9b01150.
(74) Chen, B. W. J.; Stamatakis, M.; Mavrikakis, M. Kinetic Isolation between Turnovers on Au_{18} Nanoclusters: Formic Acid Decomposition One Molecule at a Time. *ACS Catal.* **2019**, *9* (10), 9446–9457. https://doi.org/10.1021/acscatal.9b02167.